CPlantBox, a whole plant modelling framework for the simulation of water and carbon related processes

Xiao-Ran Zhou[1], Andrea Schnepf[1], Jan Vanderborght[1],
Daniel Leitner[2], André Lacointe[3], Harry Vereecken[1], Guillaume Lobet[1 *]

[1]: Agrosphäre (IBG-3), Forschungszentrum Jülich GmbH, Jülich, Germany
[2]: Simulationswerkstatt, Humboldtstraße 40, 4020 Linz, Austria
[3]: INRA, UMR 547 PIAF, F- 63100 Clermont- Ferrand, France
*: Correspond Author, Email: g.lobet@fz-juelich.de

Abstract

The interaction between carbon and flows within the vasculature is at the center of most growth and developmental processes. Understanding how these fluxes influence each other, and how they respond to heterogeneous environmental conditions, is important to answer diverse questions in agricultural and natural ecosystem sciences. However, due to the high complexity of the plant-environment system, specific tools are needed to perform such quantitative analyses.

Here we present CPlantBox, a whole plant modelling framework based on the root system model CRootBox. CPlantbox is capable of simulating the growth and development of a variety of plant architectures (root and shoot). In addition, the flexibility of CPlantBox enables its coupling with external modeling tools. Here, we connected the model to an existing mechanistic model of water and carbon flows in the plant, PiafMunch.

The usefulness of the CPlantBox modelling framework is exemplified in five case studies. Firstly, we illustrate the range of plant structures that can be simulated using CPlantBox. In the second example, we simulated diurnal carbon and water flows, which corroborates published experimental data. In the third case study, we simulated impacts of heterogeneous environment on carbon and water flows. Finally, we showed that our modelling framework can be used to fit phloem pressure and flow speed to (published) experimental data.

The CPlantBox modelling framework is open-source, highly accessible and flexible. Its aim is to provide a quantitative framework for the understanding of plant-environment interaction.

Introduction

Plants contribute for about 80% of the global earth biomass (Bar-On *et al.* 2018). They also strongly control land surface fluxes of water and carbon. Plant water uptake constitutes a major part of the evapotranspirative flux at the land surface but its prediction is extremely variable and uncertain (Trenberth *et al.* 2007; Jasechko *et al.* 2013; Vereecken *et al.* 2015). The same is true for the estimation of carbon related fluxes (Metz *et al.* 2005; Ayllón *et al.* 2018). As such, understanding the interplay between plant carbon and water flows and their environment is of importance to answer diverse questions in agricultural and natural ecosystem sciences.

The flows of water and carbon in the plant are constrained by both local and global structures (Bidel *et al.* 2000; Draye *et al.* 2010; Lobet *et al.* 2013; Fiorani and Schurr 2013). Root architecture is known to have an impact on water uptake (Lynch 2013; Lobet, Couvreur, *et al.* 2014), while shoot structure has an impact on carbon assimilation through photosynthesis (Boardman 1977; Lichtenthaler *et al.* 1981; Zhu *et al.* 2010). From an entire plant perspective, root and shoot are tightly connected, forming a complex and dynamic continuum between water and carbon flows. For instance, water availability at the root level influences carbon status in the shoot, although the physiology behind this is unclear (Hummel *et al.* 2010; Fatichi *et al.* 2019). The stomata conductance directly affects root water uptake by changing xylem pressure (Tuzet *et al.* 2003; De Schepper and Steppe 2010). Knowing the connecting structure of both shoot and root is therefore needed to better understand plant water and carbon relations.

At the organ scale, the different parts of the plant (root, stem, leaves, flowers and fruits) are connected by the vasculature, which consist of xylem and phloem vessels (fig. 1) (Jyske and Hölttä 2015; Savage *et al.* 2016). Xylem vessels transport the majority of water (Schröder *et al.* 2008; Javaux *et al.* 2008; Draye *et al.* 2010; Lobet *et al.* 2014), while phloem vessels translocate the majority of carbohydrates by pressure flow (Bidel *et al.* 2000; Van Bel 2003; Savage *et al.* 2013; De Swaef *et al.* 2015). The movement of water within the xylem vessels is typically explained by the tension-cohesion theory (Tyree 1997; Steudle 2001). This theory states that, the transpiration at the leaf level creates a tension within the xylem vessels, which is transmitted to the soil-root interface and drives the water uptake from the soil. The carbon flow in the phloem continuum is explained by the Münch theory (Münch and b. 1930; Knoblauch and Peters 2017). Briefly, Münch theory states that source organs (typically mature leaves and storage structures) load carbohydrates into the phloem sieve tubes. This strongly decreases the phloem solute water potential. Meanwhile, xylem and phloem vessels are tightly connected throughout the whole plant. This means the decreased osmotic potential in phloem will create a water flow from the xylem toward the phloem (fig. 7**C** light green line). This in turn increases water pressure in the phloem vessels, leading to a flow toward sink organs (typically roots, young leaves, flower and fruits) (roots are shown in fig. 7**C** light yellow line). (Jensen *et al.* 2012; Comtet *et al.* 2017). Recent experiments

have provided the first direct support to the Münch theory by direct measurement (Knoblauch *et al.* 2016; Savage *et al.* 2017).

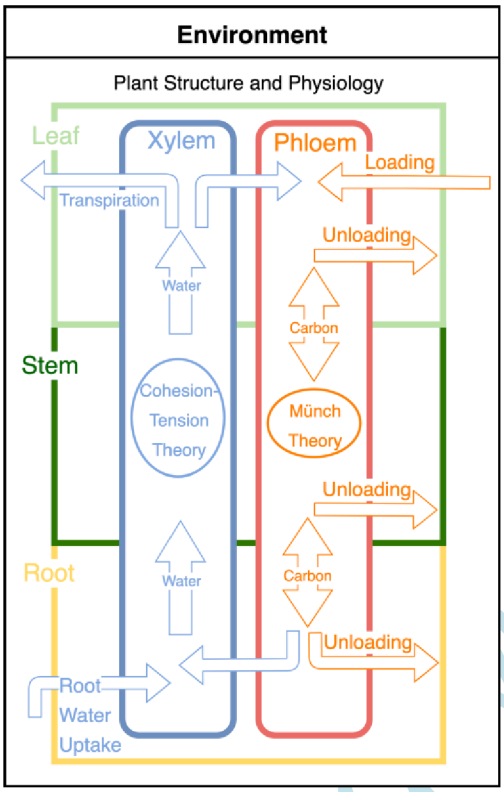

Figure 1. Structures and functions affect carbon and water flow in plants. Leaf and root contacts the environment. Xylem and phloem connect organs and exchange carbon and water.

In recent years, new phenotyping techniques (Fiorani *et al.* 2012; Lobet and Draye 2013; Rellán-Álvarez *et al.* 2015, 2016; van Dusschoten *et al.* 2016; Marshall-Colon *et al.* 2017; Hui *et al.* 2018; Zhang 2018; Lobet *et al.* 2019) have enabled the precise measurements of plant structure with high temporal and spatial resolution. However, physiological parameters, such as pressure and flows in plants are still challenging to measure. For example, the first pressure measurement in phloem sieve tubes were conducted only recently with a success rate lower than 30% (Knoblauch *et al.* 2014, 2016). Another common issue with flow and pressure data is the fragmentation of the acquired data. In other words, data can only be acquired on specific organs and at specific times, which makes it difficult to structurally understand the underlying processes. More comprehensive and quantitative studies are therefore needed to better understand the complex dynamics between the water and carbon flow within the plant, in response to heterogeneous environments (Thompson and Wolniak 2008; Mullendore *et al.* 2010).

Recently, modelling tools have been proven very useful to study water and carbon flows in plants and to analyze environmental controls on these fluxes (Fatichi *et al.* 2019; Mencuccini *et al.* 2019). In particular, Functional-Structural Plant Models (FSPMs) have a long history of simulating water or carbon flows (De Reffye and Hu 2003; Kang *et al.* 2008; Pradal *et al.*

2008; Vos *et al.* 2010; Leitner *et al.* 2010; Xu *et al.* 2011; Sievänen *et al.* 2014; Lobet, Pagès, *et al.* 2014; Zhu *et al.* 2016). Table 1 lists the most recent FSPMs simulating either the full plant structure (both root and shoot), or water and carbon flows. Among these, only a handful of 3D full plant structure models (with both 3D topology and 3D geometry) exist (Drouet and Pagès 2003; Janott *et al.* 2011; Lobet *et al.* 2012). Meanwhile, only two existing models were designed to simulate carbon and water flow simultaneously (Lacointe and Minchin 2008; Seleznyova and Hanan 2018).

We distinguish three approaches to model carbon distribution within the plant. The first approach prescribes allocation rules of assimilates between the different plant organs. The total pool of carbon is divided between different organs, which adjust their growth accordingly (Marcelis 1996; Heuvelink 1996). Usually, models using such approach do not need a fast-computational method to distribute the carbon. A second approach uses detailed mechanistic relationships to simulate carbon (and sometimes water) flow within a simplified structure. These lumped models often only represent the plant as a small set of objects (fig. 2**B**) (Steppe *et al.* 2015; De Swaef *et al.* 2015). Finally, a third approach resolves carbon and water flow within a 3D structure based on mechanistic relations between the different organs. Although these models (Bidel *et al.* 2000; Lopez *et al.* 2008; Lacointe and Minchin 2008; Seleznyova and Hanan 2018) can be computationally very intensive, they open the way to more complex representation of the plant-environment system.

Here we introduce a new functional-structural whole plant modelling framework. Inside this framework, CPlantBox and functional model, such as PiafMunch. The novelty of CPlantBox is twofold. Firstly, CPlantBox can simulate the full plant structure at vegetative growth as a single topological network of organs (both root and shoot). The simulated plant architecture is composed of nodes or coordinates, then the nodes' properties and interactions scaled up to form the network. Secondly, CPlantBox provides a framework to couple with external models. In this paper, the framework provides the interface with the carbon and water flow model, PiafMunch (Website1, PiafMunch is available upon request by contacting coauthor André Lacointe) (Lacointe and Minchin 2008; Minchin and Lacointe 2017). The coupling of CPlantBox and PiafMunch (called CPlantBox-PiafMunch in the later text) enables fast simulations on large or complex plant structures, which was difficult to achieve before (PiafMunch uses manually defined plant architecture). Previously, PiafMunch was already able to simulate simple 3D plant topology. Now, by coupling with CPlantBox, an additional 3D geometry layer is added to PiafMunch. Here we demonstrate the capabilities of the coupled model to generate a variety of plant structures and to reproduce realistic water and carbon flow behaviours.

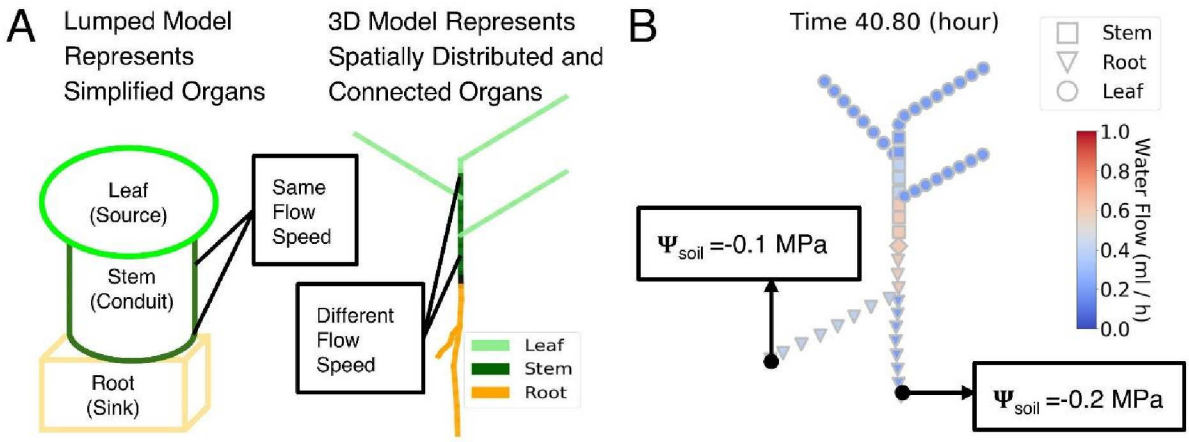

Figure 2. **A**: The flow rate in lumped model depends only on the radius of the segment. In 3D models, branching structures affect flows as well. **B**: On 3D structures, the heterogeneous soil water potential affect xylem water flows. Root in wet soil has more water flow compared to root in dry soil.

Table 1. Overview of recent 3D topology and 3D geometry whole plant (shoot and root) FSPMs

Model Name	Authors	Structure	Species	Flow(s)	Availability	Interface
GRAAL[1]	(Drouet and Pagès 2003)	3D full plant	Maize	Water	-	GUI
PlaNet-Maize[1]	(Lobet *et al.* 2012)	3D full plant	Maize	Water	Open source	GUI, Web interface
-[2]	(Seleznyova and Hanan 2018)	3D full plant topology	Small plants	Water and carbon	-	-
L-Peach	(Da Silva *et al.* 2014)	3D full plant topology	Peach	Carbon	-	-
AmapSim	(Barczi *et al.* 2008)	3D shoot or root	Generic	Water or carbon (by coupling)	-	-
Piaf-Munch[2]	(Lacointe and Minchin 2008)	3D full plant topology	Small plants	Water and carbon	Upon request	GUI, Command Line.
-[2]	(Janott *et al.* 2011)	3D full plant topology	Generic	Water	Upon request	-
This work[1]		3D full plant	Generic	Water and carbon (by coupling)	Open source	GUI, iPython notebook, Web interface

[1]: Models with both 3D topology and 3D geometry.
[2]: Models simulate interactions between carbon and water.

Material and methods

Description of CPlantBox

CPlantBox is an extension of the model CRootBox (Schnepf *et al.* 2018). CRootBox is a fast and flexible FSPM focusing on root architecture and root-soil-interaction. We took advantage of the object-oriented structure of CRootBox to add new modules to represent the different shoot organs (fig. 3**B**). The main extensions in CPlantBox are:

- CPlantBox can simulate realistic plant shoots and roots as a single connected network. The output can be coupled with water and carbon flow simulations (fig. 3**C**, **D**).

- As we move from root simulation to a full plant simulation (fig. 3**B**), more complex relationships between the different organs have been included in the model. For instance, roots can now grow from seed, roots or shoot organs (fig. 3**B**).

- The input parameter files are now XML-based (fig. 3**A**). Comparing to plain-text parameters, XML increases the robustness, flexibility (more parameters for the shoot) and readability. Backward compatibility with previous parameter file (from CRootBox) was insured.

The output of CPlantBox is a 1-dimensional network (with 3D geometry coordinates) (fig. 3**C**). Each node of the network has 3D (3-dimensional) coordinates and other properties, such as an *organtype* (which indicates if it belongs to root, stem or leaf), a radius (or width) and a water potential *etc.* The output format of the structure includes RSML (Lobet *et al.* 2015), VTP (Ahrens *et al.* 2005) and PiafMunch input format. After the plant structure is simulated (fig. 3**B**, potentially thousands of segments), an input file for the PiafMunch can be generated. Afterwards, PiafMunch can be called by CPlantBox to read the input file, run simulations and generate the output files. At the end of the simulation, output files can be interpreted and visualized either internally or externally.

The current coupling is done by file-exchange and command-line-automation. Simulating the carbon and water flow within a 300-segments plant for 100 hours growth time takes around 1 minute (dependent on parameter setting) on a regular laptop (CPU: Intel Core i5-6300U 2.4GHz, RAM 8GB 2400MHz). We also created functions to run simulations in batch processes. Installation, preprocessing, post processing and visualization are exemplified in a Jupyter notebook (Website 2).

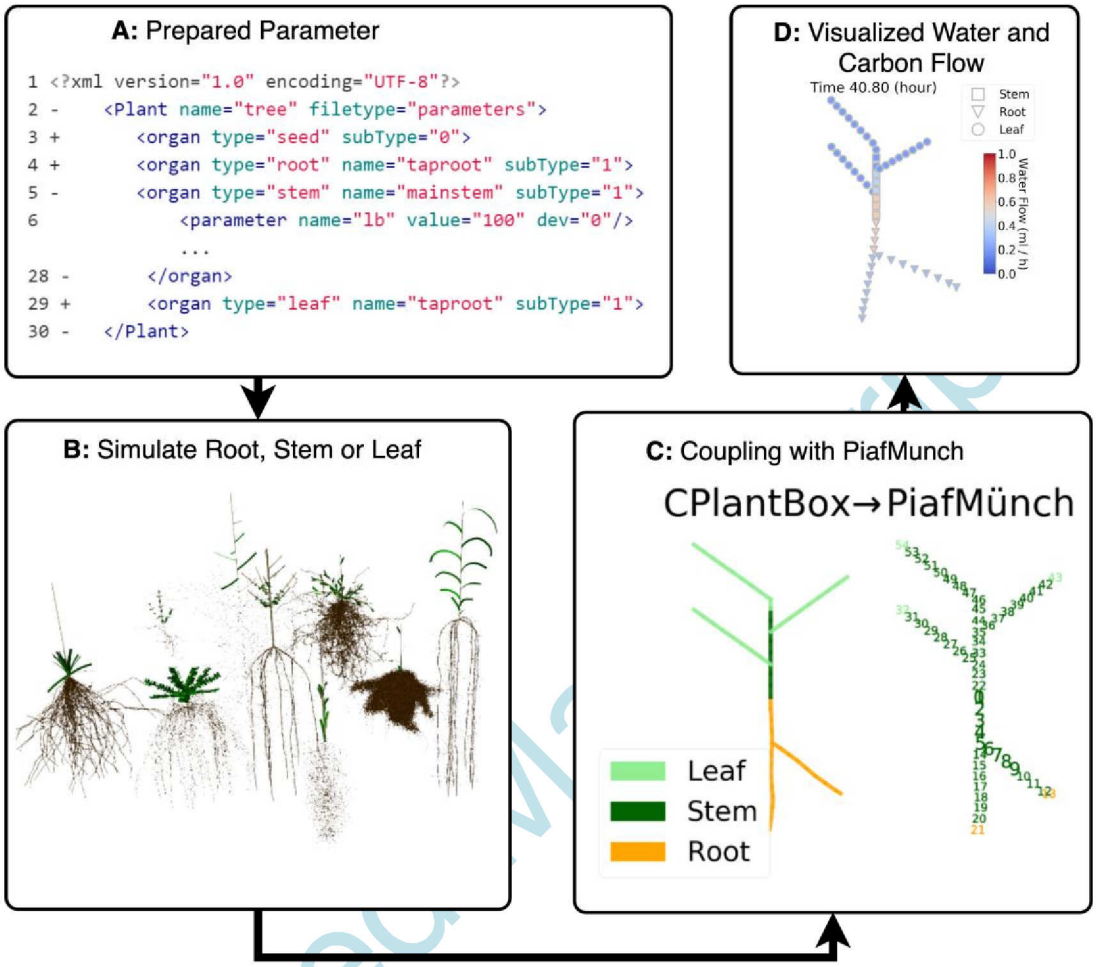

Figure 3: Flow chart of four major steps in CPlantBox-PiafMunch coupling. A: Input parameter example (organ parameters with "+" sign means it is collapsed). **B**: Output of CPlantBox is visualized. **C**: Coupling between CPlantBox and PiafMunch, where output of CPlantBox can be the input file of PiafMunch. **D**: Water flow output example from the CPlantBox-PiafMunch coupling.

Description of PiafMunch

Water and carbon flows in PiafMunch

In PiafMunch (Lacointe and Minchin 2008; Minchin and Lacointe 2017), cohesion-tension theory is a precondition of the Münch theory. The cohesion-tension theory states that xylem water flow is driven by water-potential-differences in the xylem. The water potential in general can be defined as the sum of partial water potentials: the gravimetric water potential: Ψ_z (MPa), the pressure water potential Ψ_p (MPa) and the osmotic water potential: Ψ_o (MPa). According to the cohesion-tension theory, the pressure in the water can be

smaller than zero such that a tension instead of a pressure is applied to a water body. It must be noted that the water pressure is expressed as the difference between the water pressure and the atmospheric air pressure. Following this definition, a positive pressure corresponds with a pressure in the water that is larger than the atmospheric pressure and a negative pressure with pressure that is smaller than the atmospheric air pressure. If dissolved substances flow freely within the xylem and phloem tissues, a gradient in concentrations or corresponding osmotic water potentials will not drive a flow within these tissues. Thus, the volume flow between two connected xylem's n^{th} and $(n+1)^{th}$ segments ($J_{w\_xyl,n,n+1}$ mL h^{-1}) can be written as:

$$J_{\mathrm{w\_xyl},n,n+1} = \frac{\Delta P_{\mathrm{xyl},n,n+1}}{\mathrm{r}_{\mathrm{xyl},n,n+1}} \quad (1)$$

where $r_{xyl,n,n+1}$ (MPa h mL^{-1}) is the xylem resistance and $\Delta P_{xyl,n,n+1} = (\Psi_{z\_xyl,n} + \Psi_{p\_xyl,n}) - (\Psi_{z\_xyl,n+1} + \Psi_{p\_xyl,n+1})$, $\Delta P_{xyl,n,n+1}$ is the difference between the sum of pressure and gravimetric potentials at the $(n+1)^{th}$ and n^{th} segments respectively. Similarly, the volume flow between two connected phloem sieve tubes $J_{w\_st,n,n+1}$ is:

$$J_{\mathrm{w\_st},n,n+1} = \frac{\Delta P_{\mathrm{st},n,n+1}}{\mathrm{r}_{\mathrm{st},n,n+1}} \quad (2)$$

where $r_{st\_n,n+1}$ (MPa h mL^{-1}) is the total sieve tube (include sieve plate) resistance between n^{th} and $(n+1)^{th}$ segment and $\Delta P_{st\_n,n+1} = (\Psi_{z\_st,n} + \Psi_{p\_st,n}) - (\Psi_{z\_st,n+1} + \Psi_{p\_st,n+1})$, $\Delta P_{st\_n,n+1}$ is the total potential difference between the neighbouring sieve tube segments n^{th} and $(n+1)^{th}$. At the n^{th} segment, the volume flow between the neighbouring xylem and phloem, which are separated by a semipermeable membrane, $J_{w\_lat,n}$ can be written as:

$$J_{\mathrm{w\_lat},n} = \frac{\left(\Psi_{\mathrm{p\_xyl},n} + \Psi_{\mathrm{o\_xyl},n}\right) - \left(\Psi_{\mathrm{p\_st},n} + \Psi_{\mathrm{o\_st},n}\right)}{\mathrm{r}_{\mathrm{lat},n}} \quad (3)$$

where $\Psi_{p\_xyl,n}$ is the water pressure potential in xylem and $\Psi_{p\_st,n}$ is the water pressure potential in sieve tubes, $\Psi_{o\_xyl,n}$ is the osmotic water potential in xylem and $\Psi_{p\_st,n}$ is the osmotic water potential in sieve tubes, $r_{lat,n}$ is the resistance of the membrane between xylem and phloem. Here, we should notice that, at the source location, osmotic pressure drives the $J_{w\_lat,n}$. But, at the sink location, the driving force is mainly the pressure water potential, because most osmotic water potential is removed by the unloading of carbon. The water mass balance of xylem is:

$$\Delta J_{\mathrm{w\_xyl},n} + J_{\mathrm{w\_lat},n} = 0 \quad (4)$$

where $\Delta J_{w\_xyl,n}$ is the xylem water flux divergence, either depletion or accumulation, over segment n. $J_{w\_lat,n}$ is the xylem water flux exchange between phloem. The xylem water divergence can be written as $\Delta J_{w\_xyl,n} = J_{w\_xyl,n,n+1} - J_{w\_xyl,n-1,n}$. The depletion of xylem water occurs at the source, often the leaves, where water transpired into the atmosphere or goes to phloem ($J_{w\_lat,n}$). The accumulation occurs at the sink, often the roots, where water comes from the soil or the phloem ($J_{w\_lat,n}$). Similarly, the water mass balance of phloem can be written as:

$$\Delta J_{\mathrm{w\_st},n} - J_{\mathrm{w\_lat},n} - NZS_n = 0 \quad (5)$$

Where $\Delta J_{w\_st,n} = J_{w\_st,n,n+1} - J_{w\_st,n-1,n}$ is the flux divergence, either depletion or accumulation, over phloem sieve-tube. The depletion of phloem sap occurs at the sink, where carbon is unloaded from the phloem and water goes back to xylem. The accumulation occurs at the source, where water goes from xylem to phloem and carbon is loaded to the phloem. NZS_n is the non-zero sugar volume flow accompanying $J_{s\_lat,n}$. At the source location, $NZS_n = \bar{V} \cdot J_{s\_loading,n}$, $\bar{V}$ is the non-zero partial molar volume of sucrose, $J_{s\_loading,n}$ (mmol h^{-1}) is the loading rate from the source tissue (e.g. parenchyma) to the phloem at the n^{th} node. At the sink location, $NZS_n = -\bar{V} \cdot J_{s\_unloading,n}$, $J_{s\_unloading,n}$ (mmol h^{-1}) is the loading rate from the phloem to the sink tissue.
The mass balance of sucrose can be written as:

$$J_{s\_(un)loading} + J_{w\_st,n-1,n} \cdot C_{st,n-1} - J_{w\_st,n,n+1} \cdot C_{st,n} = 0 \quad (6)$$

where, $J_{s\_(un)loading}$ is the source (sink) term. It could be zero at transportation segments, or positive value at source or negative value at sink. $C_{st,n-1}$ is the sucrose concentration at the $(n-1)^{th}$ node, the concentration multiplied by $J_{w\_st,n-1,n}$, which is the phloem (or sieve tube) flow from $(n-1)^{th}$ node to the n^{th} node, will give us the carbon mass increase from $(n-1)^{th}$ node to the n^{th} node. The $C_{st,n}$, which is the sucrose concentration in the n^{th} node, multiplied by $J_{w\_st,n,n+1}$, which is the phloem (sieve-tube) solute flow from n^{th} segment to the $(n+1)^{th}$ segment, will give us the carbon mass loss from n^{th} segment to the $(n+1)^{th}$ segment.

Comparison with experimental results

Recently, Knoblauch et al. experimentally tested the Münch theory on morning glory (*Ipomoea nil*) (Knoblauch *et al.* 2016). To validate the functions of CPlantBox-PiafMuch and estimate carbon loading/unloading speed, we decided to perform a re-analysis of their experimental dataset (measurements are shown in Table 2). In particular, we used one set of morning glory experimental data (left column of 7.5m-morning-glory in Table 2) for calibration and another set (right column of 7.5m-morning-glory in Table 2) for validation of our modelling system. We choose to use these datasets for different reasons. Firstly, the experimental measurements match almost directly both the input and output of the CPlantBox-PiafMunch model (fig. 4). Secondly, the authors performed a variety of experimental treatments, allowing us to parametrize our model on one experiment and validate on the others. Finally, the relatively simple architecture of the morning glory allowed us to focus our analysis on the resolution of carbon and water flow themselves, not the architecture

In a first experiment (that we used for the parameterization of our simulations is shown in Table 2 and illustrated in fig. 10**A**), the authors measured the permeability of sieve tubes at three locations (1 m, 4 m and 7 m) on a 7.5 m tall morning glory (referred to as 7.5 m plant in following text). The phloem pressure and phloem flow rates were also measured in the same plant.

In a second experiment (that we used for validation shown in Table 2 and illustrated in figure 10**B**), another morning glory plant was continuously defoliated except for the top four meters

(this plant is referred to as *defoliated plant*). When the defoliated stem was 2.5 m, 3.5 m, 9 m, 10 and 14 m long during its growth, the pressure of the bottom leaf was measured.

Details about the exact data transformations performed between the experimental measurements and the model parameters can be found in the Supplementary material 1.

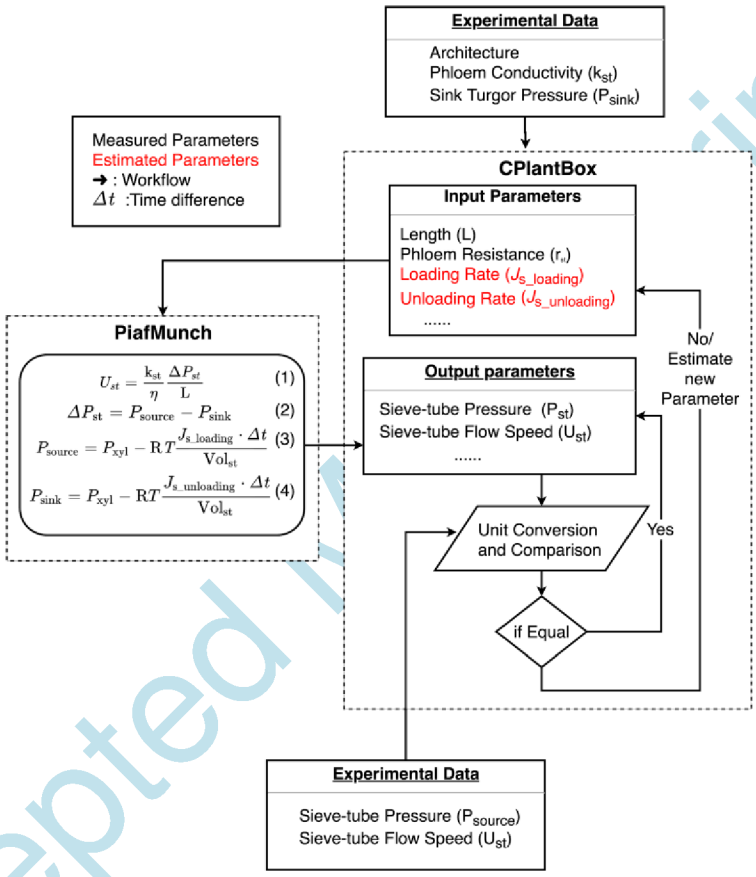

Figure 4. Measured parameters (in black text) and estimated parameter (in red text) in comparison with experiment. Length is calculated from simulated architecture (left side of fig. 10 **A**, **B**), which is based on the schematic drawing (right side of fig. 10**A**, **B**). r_{st} is converted from measured k_{st} (Supplement I, Equation 7). Pressure difference (ΔP_{st}) is the phloem source pressure (P_{source}) minus phloem sink pressure (P_{sink}). R is the universal gas constant and T is the absolute temperature. P_{xyl} is the pressure of xylem at source or sink location, those pressures are calculated by carbon loading rate ($J_{s\_loading}$) and carbon unloading rate ($J_{s\_unloading}$). Arrows highlight our modelling workflow. ΔT is the time difference, Vol_{st} is the sieve tube volume. Units are in Table 3 and Supplemental material 1. The fitting of loading and unloading rate to source phloem pressure and flow rate are shown at the end of supplemental material 1.

Table 2. List of experimental measurements done by (Knoblauch *et al.* 2016), other parameters used for simulation are summarized in Table 3.

Measurements	**Measurements on 7.5 m morning glory**	**Measurements on defoliated morning glory**
Architecture	Idealized schematic drawing (fig. 10**A**)	Idealized schematic drawing (fig. 10**B**)
Sieve-tube conductivity (k_{st})	At 1 m, 4 m and 7 m location	When plant is 18 m long
Pressure (P)	Leaf phloem turgor pressure is measured at 1st, 3rd, 5th, 9th and 10th leaf (blue dots in fig. 10**C**). Root turgor pressure is measured in the cortex of elongation zone.	Leaf phloem turgor pressure is measured at bottom leaf of the 4 m foliated stem when plant is 2.5 m, 3.5 m, 9 m, 10 and 14 m long (blue dots in fig. 10**D**)
Phloem Sieve-tube Flow Speed (U_{st})	Between 2nd and 3rd leaf (arrows in fig. 10**C**)	When plant is 18 m long
Viscosity (η)	Assume constant at 1.7 mPas	Assume constant at 1.7 mPas

Results

In the following section, five functions of CPlantBox are exemplified and the results created by those functions are showcased. Structurally, a wide variety of whole plant architectures are simulated by CPlantBox in example 1. Functionally, we evaluated water and carbon simulations of a three-leaf-two-root plant under either homogeneous or heterogeneous environments in example 2 and 3. Quantitative comparisons between simulations and experimental data are shown in example 4 and 5.

Example 1: Simulation of contrasted plant architectures with CPlantBox

Plants display a variety of forms and architectures, both above and below ground (Barthélémy and Caraglio 2007). Stem branching patterns are important factors determining the above-ground architecture of plants. Fig. 5**A** shows an example of three branching patterns generated by CPlantBox using different parameter files. A second important determinant of the above-ground architecture is the arrangement of the leaves on the stems. Fig. 5**B** includes three leaf arrangements created by only changing single input parameter. By combining different branching patterns and leaf arrangements, we extended existing CRootBox outputs (Schnepf *et al.* 2018) into full plant architectures (fig. 6). It is worth mentioning here that each unique structure is obtained solely by changing the input

parameter files. The source code itself is not modified. This level of flexibility is more friendly to the end-users.

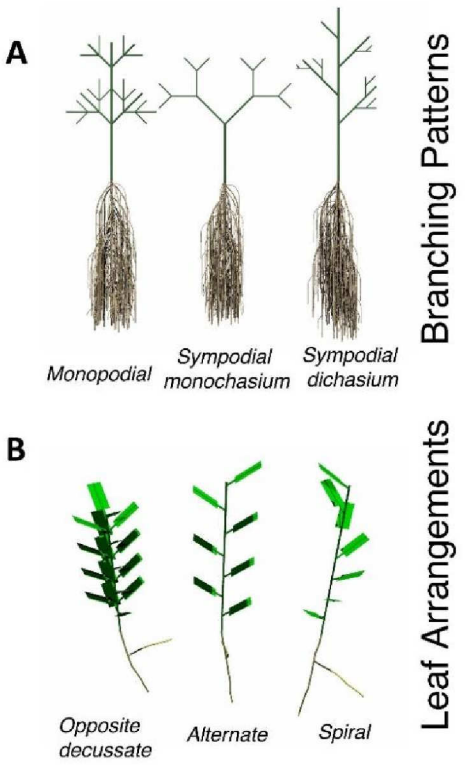

Figure 5: A: Simulated stem branching pattern simulated by CPlantBox; **B**: leaf arrangements simulated by CPlantBox

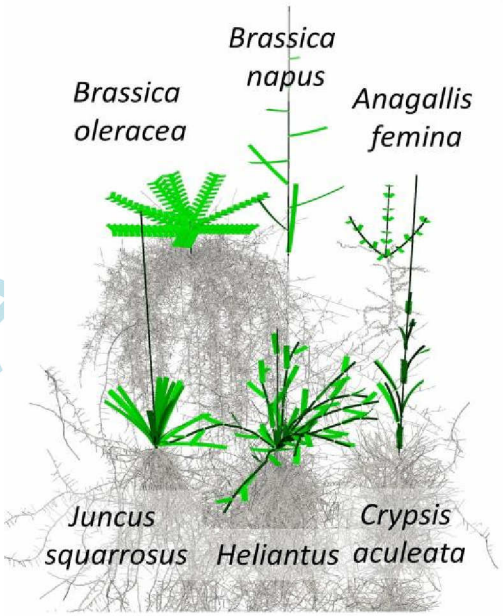

Figure 6: Simulated whole plant structures. *Brassica oleracea, Brassica napus, Anagallis femina, Juncus squarrosus, Heliantus* and *Crypsis aculeata.*

Example 2: Simulation of water and carbon flow with the coupled model CPlantBox - PiafMunch

We created a small plant (three leaves and two roots) to simulate carbon and water flow (figs. 3**C** and 3**D**). The input and output parameters values were collected from various sources from the literature (summarized in Table 3) (Zwieniecki *et al.* 2001). The simulated values of xylem pressure, flow rate and hydraulic conductivities are within the range of literature values. For example, xylem can sustain flow under pressure between -2.0 to -8.0 MPa, before losing 50% of its conductivity (Martínez-Vilalta *et al.* 2002). The simulated xylem water flow rate is typically around 1 ml h^{-1}.

The transpiration rate on each leaf was set to mimic diurnal flow patterns. We set the transpiration rate to 0.2 mmol h^{-1} (0.0036 ml h^{-1}) per leaf during daytime (from 5:00 to 17:30), and to 0 at nighttime (from 17:30 to 5:00 the next day). As shown in fig. 7**A**, pressure is decreasing from root to leaf. Xylem flow during the day is caused by transpiration, and the waterflow going back into the xylem caused the xylem flow at night (which are lower than 0.0005 ml h^{-1}, can be visible when zoom in fig. 7**B**). There are water moving from xylem to phloem at the source. Indeed, as the carbon is loaded into the phloem, it reduces the sieve tube water potential. The water crosses the membrane and moves from xylem to phloem. Therefore, we can observe that phloem carbon flow rates are affected by the diurnal xylem water flow (fig. 7**D**).

The loading rate into the phloem at source location is set to a constant value during both day and night. This is consistent with experimental data (Stitt *et al.* 2010; Streb and Zeeman 2012; Pokhilko and Ebenhöh 2015), as starch is degraded at night and the generated sucrose can be loaded into the phloem to sustain the flow.

Table 3: Literature values and simulation parameter values used for small plant, 7.5 m plant and *defoliated plant*.

Parameter	Symbol	Type	Experimental Range	Unit	Small Plant	7.5 m Plant	Defoliated Plant
Xylem[1] Resistance	r_{xyl}	Input	0.011 to 3.3 by Stem (Sellin 1993)	MPa h mL^{-1}	2.08 by Stem 6.9×10^{-2} by Segment (0.25cm)	0.081 by Stem 0.0005 by Segment (5cm)	0.071 to 0.191 by Stem 0.0005 by Segment (5cm)
Phloem[2] Resistance	r_{phl}	Input	40 to 90 (Knoblauch *et al.* 2016)	MPa h mL^{-1}	70 by segment (0.25 cm)	Supplement Material I fig. 13	Supplement Material I fig. 13
Transpiration[1]	-	Input	0 to 1 × 10^6 m^{-2} (Wullschleger *et al.* 2000; Almeida *et al.* 2007)	mmol h^{-1}	0.2 or diurnal	0.2	0.2
Soil Water[2] Potential	-	Input	-0.2 to -0.8 (Draye *et al.* 2010; Lobet, Couvreur, *et al.* 2014)	MPa	-0.6	-0.6	-0.6
Loading Rate[3]	$J_{s\_loading}$	Input	--	mmol h^{-1}	0.0007 on each source segment	6.4×10^{-6} on each source segment	6.4×10^{-6} on each source segment
Unloading[3] Rate	$J_{s\_unloading}$	Input	--	mmol h^{-1}	0.00028 × C_{st}^4	0.012 × C_{st}^4	0.012 × C_{st}^4
Xylem[1] Pressure	P_{xyl}	Output	-0.2 to -8 (Martínez-Vilalta *et al.* 2002)	MPa	0 to -0.7	0 to -0.7	0 to -0.7
Phloem[2] Pressure	P_{phl}	Output	0 to 1.44 (Savage *et al.* 2017)	MPa	0 to 1.8	0 to 1.4	0 to 1.8
Xylem Water[1] Flow Rate	J_{w_xyl}	Output	0 to 3.6 (Zwieniecki *et al.* 2001)	mL h^{-1}	0.20 to 0.62	0 to 1.2	0 to 1.2
Phloem Solut[2] Flow Rate	J_{w_st}	Output	-0.02 to 0.02 (Windt *et al.* 2006; Comtet *et al.* 2017)	mL h^{-1}	-0.001 to 0.0006	-0.002 to 0.0006	-0.002 to 0.0006
Phloem[2] Carbon Flow Rate	J_{s_st}	Output	--	mmol h^{-1}	0 to 0.00022	0 to 0.00022	0 to 0.00022

[1] Estimated Input parameters that falls into literature range.

[2] Parameters equal to Knoblauch's measurements.

[3] Calibrated parameters through Knoblauch's 7.5m-plant measurements, unchanged on defoliated-plants.

[4] C_{st}: Carbon contraction in sieve tubes (details in Supplemental material 1, Equation 11).

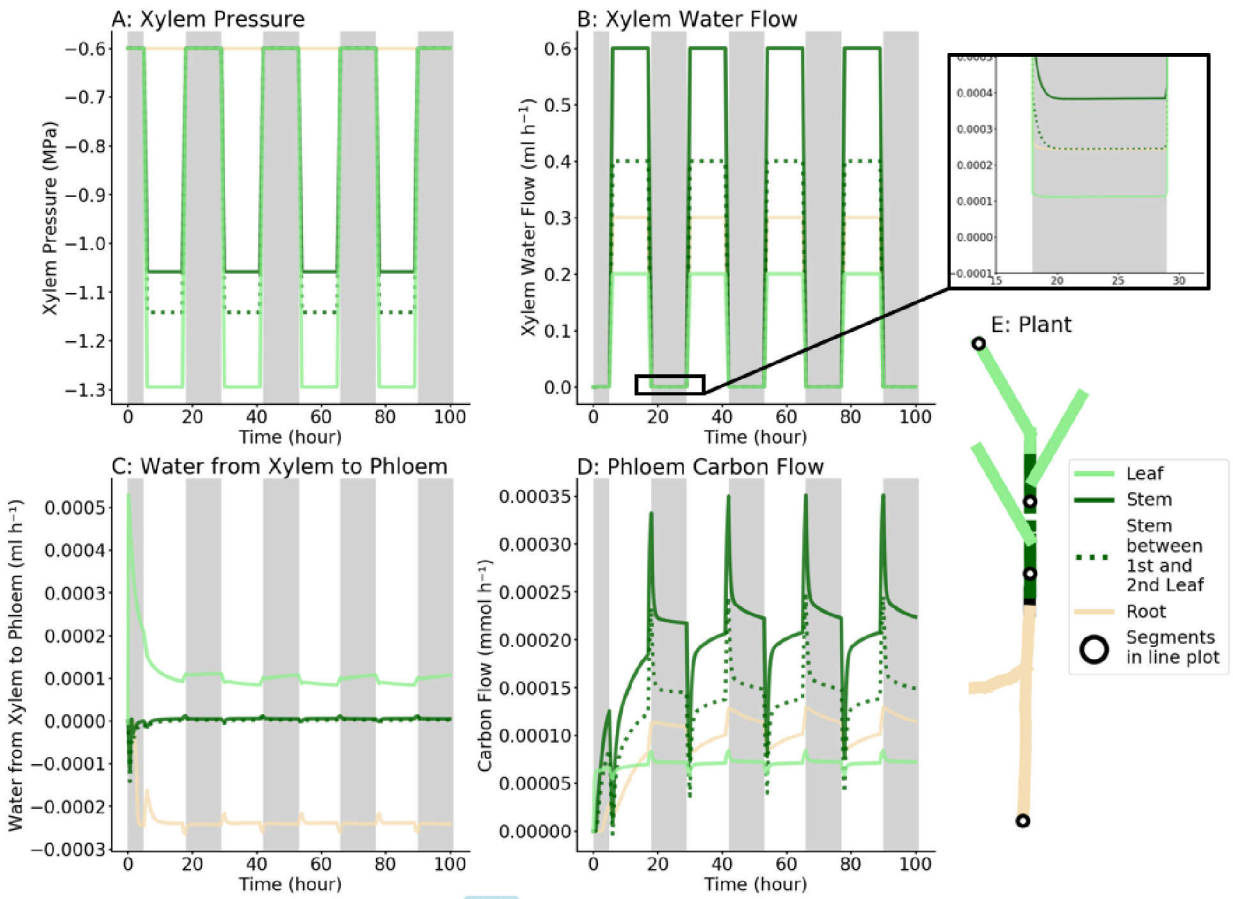

Figure 7 A: Transpiration creates xylem pressure gradients during the day, whereas the pressure remains comparatively stable during the night. **B**: The pressure gradient caused xylem water flow during daytime, the water flow at night is low, it is the water flow from phloem to xylem. **C**: The water flows from xylem to phloem at source location, whereas it flows from phloem to xylem at sink location. **D**: Phloem (sieve-tube) carbon flow fluctuations are caused by diurnal xylem water flow, the trend of changing is qualitatively consistent with previous studies (Stitt *et al.* 2010; Streb and Zeeman 2012; Pokhilko and Ebenhöh 2015); **E**: Plant structure where the colors correspond to the flow figures from **A** to **D**, the dashed line shows the segments between the first and second bottom leaves. The flows going to circled segments are also shown as dashed lines in **B** and **D**. The pressure or flow exchanges of the circled segments are shown in **A** and **C.** The loading rate inside the phloem at source location is set to constant during both day and night, because starch is degraded to sucrose and then loaded into the phloem at night (Stitt *et al.* 2010; Streb and Zeeman 2012; Pokhilko and Ebenhöh 2015).

Example 3: Simulations of water and carbon flows in response to heterogeneous environments.

Heterogeneous environments can have a large impact on plant growth and development. 4D FSPM can be used to simulate and visualize such environmental impact. To observe the effect

of heterogeneous soil water availability on the carbon flow within the root system, we manually assigned two different soil water potentials at two root tips (bottom root in blue color with -0.2 MPa, upper root in red color with -0.4 MPa in fig. 8**A**). In fig. 8**B**, we observe a pressure difference between two roots, which causes hydraulic redistribution at night from the wet to the dry parts of the root system (fig. 8**C**). During the day, the water flow to the wet part is larger than the flow to the root in the dry soil. We also observed that the carbon concentration in the high water potential root is lower (red line in fig. 8**D**). In fig. 8**F,** we can see that total carbon flow in wet root is lower than the flow in the dry root.

Different temperature or developmental stages can also cause heterogeneous leaf transpiration rate. We assigned the 0.3 mmol h^{-1} (0.0054 ml h^{-1}) transpiration on the top left leaf (higher transpiration leaf in fig. 9**A** with red color), 0.2 mmol h^{-1} (0.0036 ml h^{-1})transpiration on the right leaf (middle transpiration leaf in fig. 9**A** with green color), 0.1 mmol h^{-1} (0.0018 ml h^{-1}) transpiration on the bottom left leaf (lower transpiration leaf in fig. 9**A** with blue color). In fig. 9**B** and **C** we can observe the pressure and flow gradient of three leaves at different transpiration rate. In fig. 9**D** and 9**E**, we observe that carbon concentrations are different, but total carbon flows are only slightly different between the different leaves as loading rate is kept constant. In fig. 9**F**, we can see that, when transpiration changes between day and night, the carbon flow in high transpiration leaf is more sensitive to the changes. However, the total carbon flow did not change significantly. In this example we kept the loading and unloading speed homogeneous and constant. It is because physiologically the starch degradation will compensate a temporal loss on the leaf level, just the same as the night carbon loading (Zhang *et al.* 2016; Savage *et al.* 2016). The carbon loading is likely to decrease in the long term, but it might not take effect in a few days.

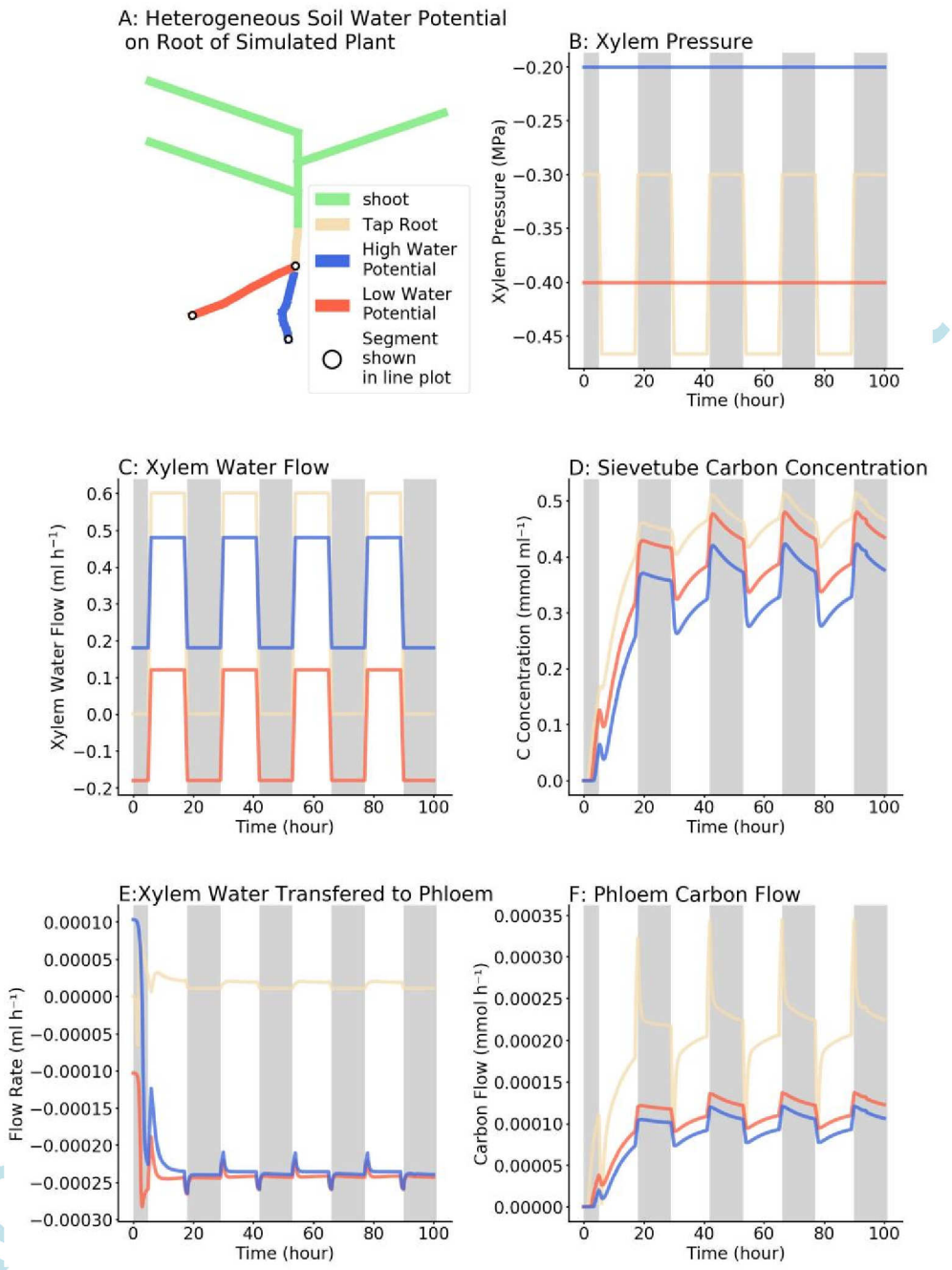

Figure 8. A: Soil water potential around the lower root (blue color) is higher than the upper root (red color). **B:** Pressure values at the boundary location are different according to the higher or lower soil water potential **C**: The bottom root (blue color, in wet soil) xylem, has higher water flow. The flow rate in upper root (red color) is negative at night. it means that, at night the water is coming out from the upper root to the soil, which is also called the hydraulic redistribution (in other words, the plant root system behaves as a pathway for water flow from wet to dry (or salty) soil areas). **D:** Carbon concentration in the dry (upper) root is higher than the wet root. **E**: Water flows from xylem to phloem at sink location only in the wet root (blue line) shortly at the beginning, then water flows from phloem to xylem in both roots at a similar rate. **F**: Carbon flow decreased in the high water potential (lower) root phloem.

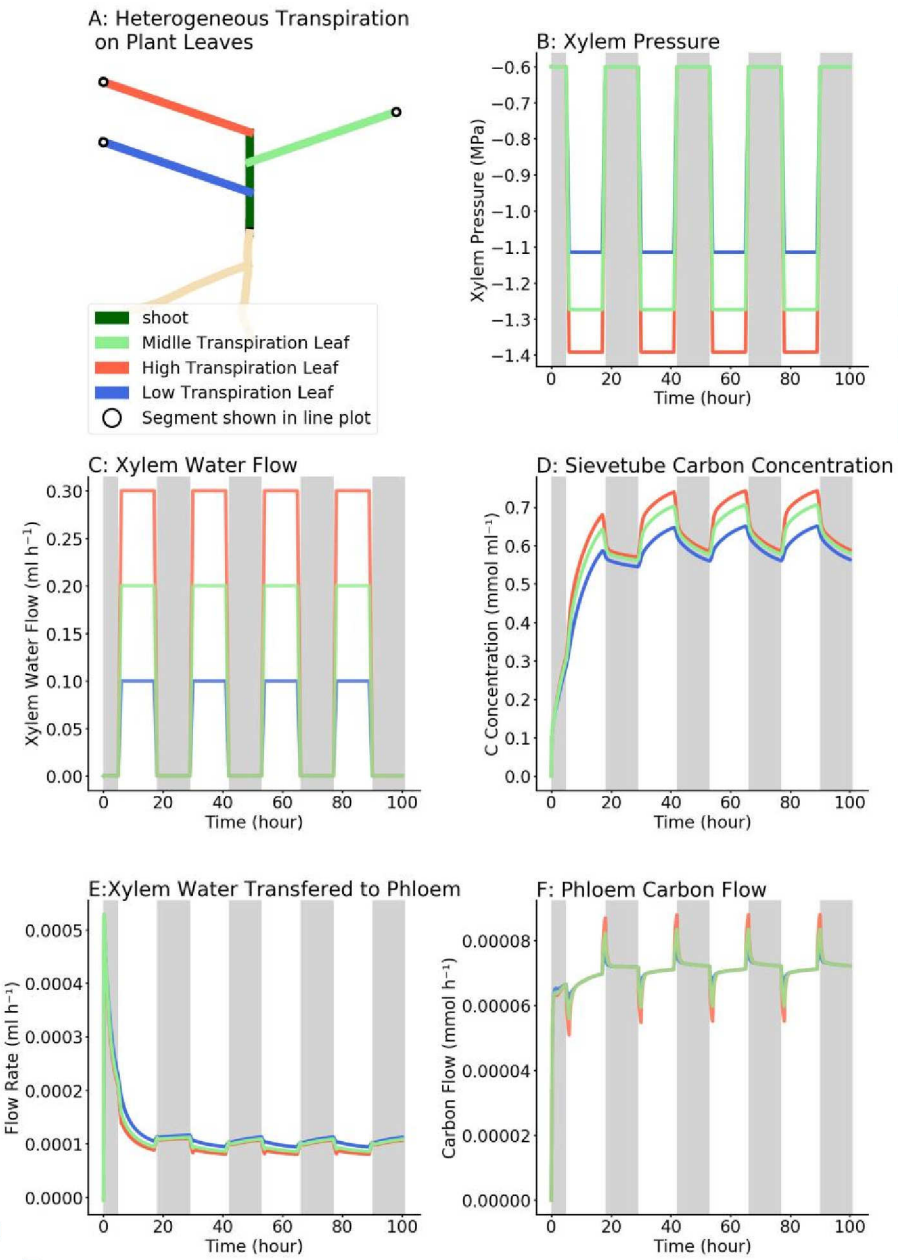

Figure 9. A: The lower left leaf (in blue) has lower transpiration rate and the top left leaf (in red) has higher transpiration rate. **B:** The pressure in each leaf is changed according to their transpiration rate. **C:** The water flow in each leaf is changed according to the transpiration rate. **D**: Carbon concentration on the higher transpiration leaf (red line) is higher. **B**: Water going from xylem to phloem at source location is lower at the higher transpiration leaf (red line). **F**: Carbon flow rates are the same at steady status, leave with higher water transpiration (red line) are more sensitive to the changes.

Example 4: Predicting carbon loading and unloading for contrasted morning glory shoot architectures in morning glory

To assess whether CPlantBox-PiafMunch was able to simulate realistic carbon and water flow values, we simulated experiments conducted with morning glory (Knoblauch *et al.*

2016). In order to simulate Knoblauch et al.'s experimental results on the morning glory, six virtual plants with contrasted architectures were created (fig 10). The architecture's parameterization is based on the idealized schematic of the original paper. As described in Table 2, the reference plant was 7.5 meters long, with 12 homogeneously distributed leaves and one shoot tip (fig. 10**A**). The *defoliated plants* each had four leaves and one shoot tip near the apex of the stem, with different length for the defoliated section (fig.10**B**).

Regarding the physiological parameterization for the carbon and water flow simulation, in both the experiments and the modelling exercise, the morning glory was simplified to 1-source-1-sink system. Therefore, we assumed that the 12 leaves and the shoot tip are all homogeneous sources with the same carbon loading rate. The carbon unloading rates in the sinks were also considered homogeneous. Thus, we could create a 1-source-1-sink scenario as shown in fig. 10**C**, where all leaves together are counted as one source and all the roots together count as one sink.

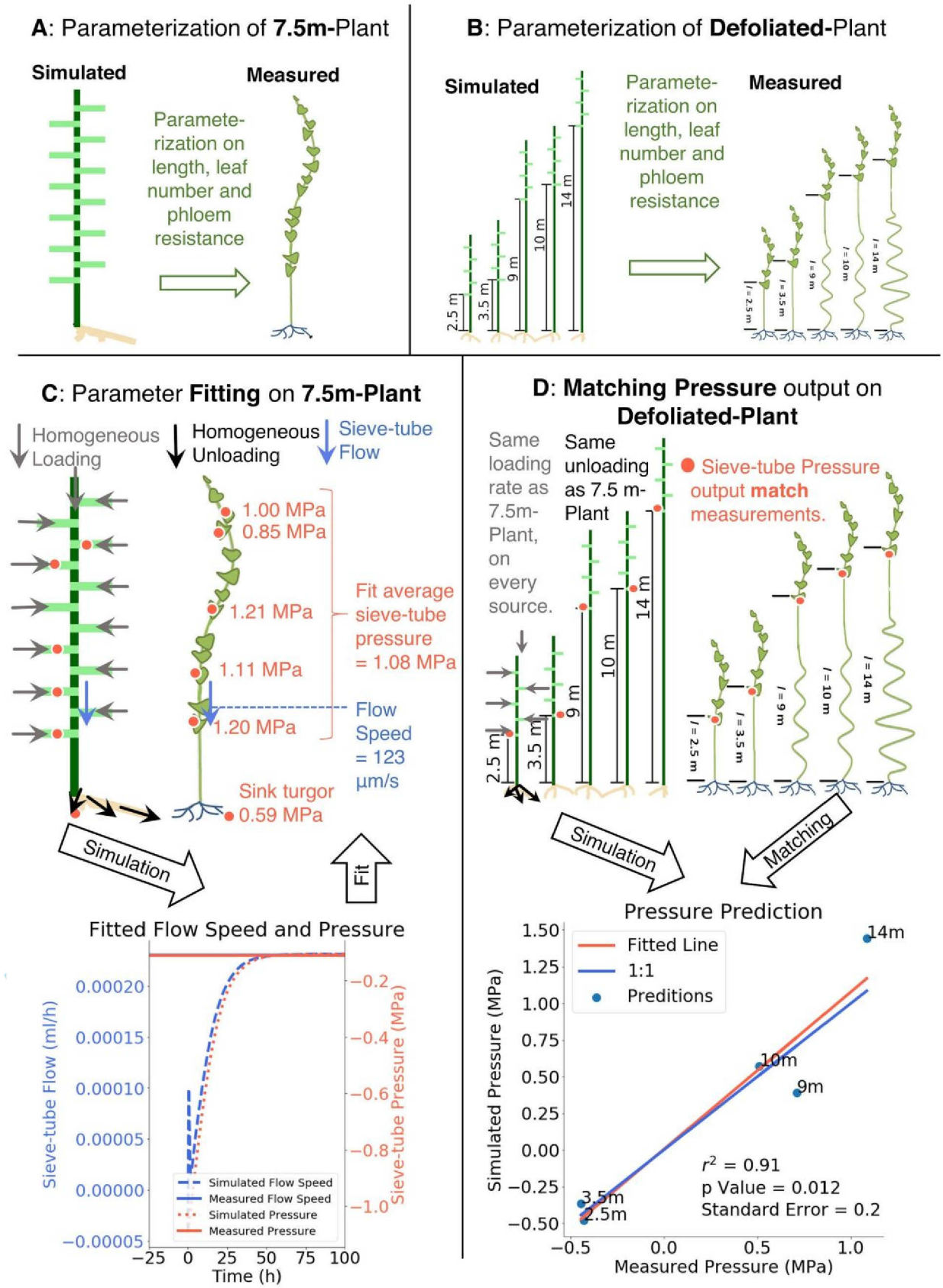

Figure 10: Steps of comparisons between simulations and experiments. **A:** one *in silico* plant

structure (left) is created based on schematic drawing of the *7.5m-plant* (also shown in Supplemental material 1 fig. S2). The resistance parameterization can be found on Supplemental material 1, fig. S1. **B:** five *in silico* plant structures are created based on schematic drawing of *defoliated plant*. **C:** In phloem, physiological parameters such as source average pressure (red) and sieve tube flow rate (blue) are fitted by applying homogeneous loading rate (grey arrows) on each leaf, and homogeneous unloading rate (black arrows) at each root tip. Parameters can be found in Table 2, fitting of loading and unloading speed can be found in fig. 4 and supplement material table 4. **D:** By applying the fitted unloading rate and loading rate from 7.5m-Plant on five *in silico* defoliated-plants, simulated pressure values match the measured values from Knoblauch et al. (2016).

As shown in fig. 10**C** and fig. 4, we used the measured pressure and measured flow rate to find our initial input parameters, in particular the carbon loading and unloading rate. We estimated the corresponding loading and unloading rate using a least square fitting (lower part of fig. 10**C**, details are in Supplemental material 1, Table 4).

The carbon loading and unloading rate estimated on the 7.5-meter plant were then applied on the *defoliated plants* (Table 2 and fig. 10**D**). None of the parameters used in 7.5 m plant simulations were modified except the plant structure (fig. 10**B)**. As shown in fig. 10**D**, we could see that the simulated pressure values in the sieve tubes were in good agreement with the experimental values.

Example 5: Studying source-sink relations at the organ level in morning glory

In the previous section, the plant architecture was simplified to a 1-source-1-sink structure (fig. 10**C**), as same as the experimental data analysis (Knoblauch *et al.* 2016). We wondered if the model would be able to simulate the detailed relationship between different leaves inside the single source. It should be noticed that, as the large variance between the leaves might be caused by experimental variations, such detailed fitting might not be biologically relevant. However, it remains an interesting conceptual exercise, to test the flexibility and capabilities of our models.

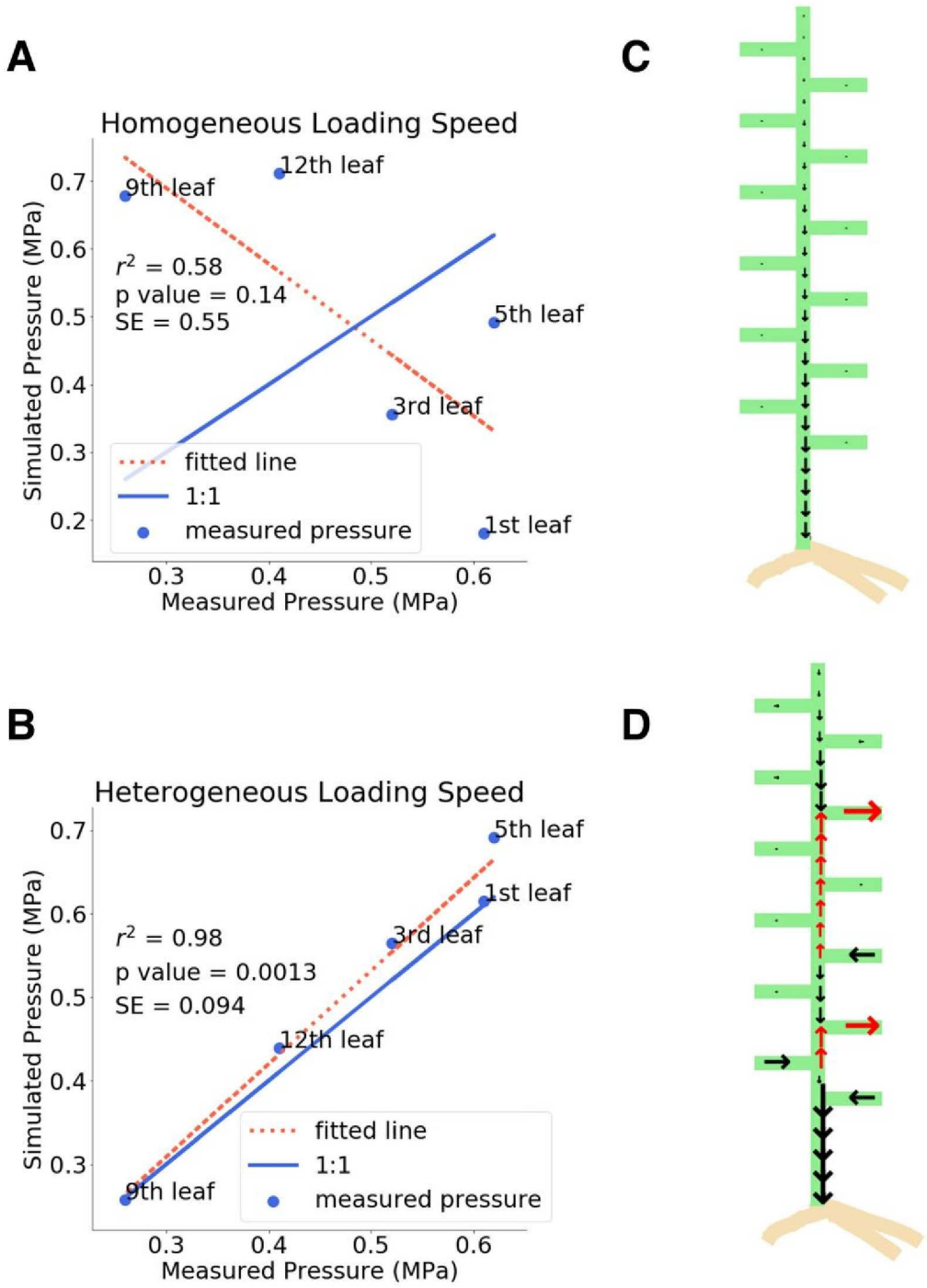

Figure 11: Comparison of simulations with (A) equal loading rate on all leaves to fit average pressure and

(B) individual loading / unloading fitted pressure on each single leaf; **A:** Result for using homogeneous loading rate on each leaf; **B:** Fitted individual loading and unloading rate on each leaf; **C:** Flows are all heading to root when all leaves are sources with same loading rate (the scenario we used for parameter fitting); **D:** Flows directions changed (in red color) when the individual leave pressure are fitted (it is only one of the possible solutions, to show that we could change loading/unloading value on each source).

We reused the calibration obtained on the 7.5 m plant (figs. 10 **A** and **C**). As shown in fig. 11**A**, it is obvious that the simulated pressure in each single leave does not fit the measured pressure. Therefore, we fitted each single leaf pressure by assigning independent carbon loading and unloading rate. We observed that, when we reached a good fit on fig. 11**B**, the directions of individual flows changed significantly compared to the flow when fitting the parameters globally (lower line plot of fig. 10**C)**. Indeed, with the individual fitting, some leaves become carbon sinks instead of being carbon sources. In fig. 11**D** the red arrows indicate a change on the carbon flow directions compared to the 1-source-1-sink scenario, as well changes in the total carbon loading (fig. 11**C**).

Discussions

CPlantBox generates full plant architectures

Historically, root and shoot models have been developed independently. Most models indeed focus on either part of the plant, representing the other one as a boundary condition. Some existing models are able to simulate both root and shoot, but for specific plant species (Drouet and Pagès 2003; Lacointe and Minchin 2008; Janott *et al.* 2011; Da Silva *et al.* 2014; Lobet, Pagès, *et al.* 2014). Here, we presented CPlantBox, the first model, to our knowledge, able to represent both root and shoot, as a single network, for a variety of plant species (see example 1 in the Results section, and figs. 5 and 6).

CPlantBox was designed to be flexible and amenable for multiple plant studies. For the root part, CPlantBox inherited the flexibility of the model it was built upon, CRootBox. As CRootBox is able to generate any type of root architecture, so is CPlantBox. For the shoot part, we implemented several branching and leaf arrangement patterns. By combining these patterns, many types of shoot architectures can be simulated. Both root and shoot architectural parameters are defined into the model parameter file, making it easy to setup and reproduce.

CPlantBox-PiafMunch simulates water and carbon flow in the full plant

We combined CPlantBox with a mechanistic model of carbon and water flow: PiafMunch (Lacointe and Minchin 2008). The coupled model allowed us to simulate water and carbon

flow within complex full plant architectures, which was not possible previously. In the results section, we demonstrated four examples. Example 1 is focusing on structures, while example 2 focuses on diurnal carbon/water flow compared to literature measurements. Example 3 shows that the combinations of structures and functions could reproduce qualitatively experiments from the literature. Example 4 reproduces the experimental results quantitatively, then in Example 5 we used conceptual experiments to prove that the heterogeneous leaf environments (in Example 3) can explain the experimental results.

In our simulations, we could observe a strong interplay between xylem and phloem flows. The diurnal transpiration patterns (the high peak in fluxes in the morning and the sharp decline when the light was stopped followed by an increase in flux during night) (fig. 7), are consistent with previous experiment and modelling (Pokhilko and Ebenhöh 2015). The low water potential in the xylem vessels during the day (as a result of the high transpiration rate) limits the water movement toward the phloem. During the night, as the stomata closes, the xylem water potential increases, leading to a higher water flow toward the phloem sieve tubes and a higher flow of carbon throughout the whole plant (fig. 7**D**). However, the higher night carbon flow might also be caused by constant loading rate, whereas in some cases, the loading rate at night is reduced to 60% of the day value (Kallarackal *et al.* 2012), so that the overall carbon flow may not be increased. In turn, the water flow from the xylem to the phloem induced a small upward water flow during the night, even in the absence of transpiration flux (fig. 7**B**). These results from our coupled models are comparable to previous published modelling results (Lacointe and Minchin 2008, 2019; Minchin and Lacointe 2017) and are consistent with experimental data (see Table 2 for details) (Thorpe *et al.* 2011).

CPlantBox-PiafMunch considers the impact of heterogeneous environments

One of the main advantages of functional-structural plant models is their ability to explicitly consider the influence of heterogeneous environments (in both space and time). In our third example, we used our coupled CPlantBox-PiafMunch modelling framework to simulate the influence of heterogeneous soil and atmospheric conditions on the carbon and water flows in the plant.

First, we imposed different soil water potentials to the different roots of our plant (fig. 8**A**). In response to this heterogeneity, we could make two main observations. Firstly, root water potential and water flow (fig. 8**B**, 8**C**) was directly influenced by the soil water potential. As the soil water potential decreases, the water flow in the xylem decreases. This is a well-known effect, observed both *in vivo* (Doussan *et al.* 2006; Garrigues *et al.* 2006) and *in silico* (Javaux *et al.* 2008; Meunier *et al.* 2016). Secondly, we observed that the carbon flow (fig. 8**F**) in the phloem was inversely correlated with the soil water potential. Indeed, our simulation results show that carbon flow is slightly higher in the portion of the root system in contact with a dry soil (red line in fig. 8**F**). This is due to the lower carbon concentration of

root phloem in wet soil (blue line in fig. 8**D**). The lower carbon concentration in wet root phloem (blue line in fig. 8**D**) is a result of dilution by water from wet root xylem to wet root phloem along the root until the root tip (like tap root in light yellow color). At the root tip, the unloading rate is proportional to the carbon concentration. Thus, the flow rates of two split root are similar. Because the flow rates are similar, but concentration is lower in the wet root, the total carbon flow is lower in the wet root (fig. 8**F**). Again, this dynamic was observed experimentally for several plant species in split root experiment (William *et al.* 1991; Farrar and Jones 2000; Muller *et al.* 2011).

To simulate heterogeneous atmospheric environment, we imposed different transpiration rates to the different leaves of our plant (fig. 9**A**). Like water potential change at the sink location, the transpiration rate at the source location directly induced changes of xylem pressure (fig. 9**B**) and xylem water flow rate (fig. 9**C**). Heterogeneous transpiration rates on leaves are also observed *in vivo* and simulated *in silico* (Sinoquet *et al.* 2001; Pincebourde *et al.* 2007). In fig. 9**D**, we could observe that the carbon concentration in phloem is increased, because in fig. 9**E** we could observe that in the high transpiration leaf (red line), less water is moving from xylem to phloem. This is because the water potential increases (red line in fig. 9**B**) and pressure drops (red line in fig 9**A**) in the high water potential leaves. Thus, the final phloem carbon flow rate did not change at steady state (lines are aggregating in fig. 9**F**)

Current limitations of the model and future perspectives

In this paper we highlighted some of the capabilities of our new coupled model CPlantBox-PiafMunch. We have shown that we can simulate realistic water and carbon flow within a full plant structure. However, it is important to stress the current limitations and future developments of our model.

Firstly, all the simulations were done with static plants. At this stage, we did not explore the impact of the carbon distribution on the growth and development of the plant. The current version of CPlantBox platform simulates the flow of carbon based on predefined unloading parameters. In future modelling project, we are planning to compute the root carbon demand on a local (segment-scale) basis. For instance, carbon transported to the root is also used for exudation and maintenance (Farrar and Jones 2000). In the future, we will explicitly connect the growth function in CPlantBox to the local carbon availability as prescribed by PiafMunch.

Secondly, in the presented simulations, the environment was static as well. In order to explore only the resolution of carbon and water within the plant, we did not connect our models to dynamic representations of the environment. In reality, the soil water potential will change rapidly if the plant transpiration is sufficient. Again, a dynamic link to environment will be done in the future, as we plan to integrate CPlantBox into the modeling framework CRootBox-DuMuX (Flemisch *et al.* 2011; Koch *et al.* 2018; Schnepf *et al.* 2018). By doing

so, we will be able to explore the feedbacks between the plant and the environment, especially soil, in a dynamic way.

Finally, in this version of the models, carbon production is prescribed at the segment or node level. Again, this what not an issue so far, as we wanted to explore the flow distribution only. However, in the near future, we plan to include leaf-level photosynthesis module (de Pury and Farquhar 1997; Farquhar *et al.* 2001), to be able to better represent the dynamic response of the plant to its changing environment.

Conclusions

Experimental measurements of carbon and water flow can be challenging, as most available measuring methods are time consuming and destructive (Knoblauch *et al.* 2014, 2016), preventing the continuous observation of these flow as the plant develops. Fortunately, models can be used as analysis tools for such complex experimental setups.

Here we have used our coupled models (CPlantBox-PiafMunch) to reverse-estimate hidden experimental parameters. For instance, by using measured carbon flow, phloem resistance and pressure, we were able to give consistent estimates of carbon loading and unloading rate in the phloem, in the different plant organs.

More generally, this is a good example of using models as complex analysis tools. As experimental setup and biological questions become more and more complex, it becomes harder to interpret the results. Models such as CPlantBox-PiafMunch can help integrate such results and place them into a whole plant perspective. Carefully using the model can then give us access to additional parameters that were not available experimentally.

Exploring the interplay between the environment, the plant architecture, and the plant water and carbon flow is experimentally challenging. Measurements take time and are often destructive. However, functional structural plant models have been shown to be able to efficiently represent plant-environment interplay *in silico*.

Here we have presented a new whole plant framework, CPlantBox. We have shown that CPlantBox is able to represent a variety of plant architectures, both root and shoot. We also connected CPlantBox to a mechanistic model carbon and water flow, PiafMunch. The coupled model was able to reproduce realistic flow behavior in complex plant structures. We were also able to use the models to reproduce experimental data and estimate hidden experimental variables.

Model and data availability

- CPlantBox is open source under GPL 3.0 license, available at https://github.com/Plant-Root-Soil-Interactions-Modelling/CPlantBox/tree/isp/
- Model parameter files are available at: http://doi.org/10.6084/m9.figshare.9785396
- PiafMunch output of simulation example 2, 3, 4 can be found here: https://figshare.com/articles/Output_of_CPlantBox-PiafMunch_coupling/9971225
- Youtube channel of simulations: https://www.youtube.com/channel/UCPK-pFfpK94jiamgwHxX32Q

Acknowledgements

We would like to show our gratitude to Xavier Draye, Mathieu Javaux, Michael Knoblauch, Clément Saint Cast for sharing their pearls of wisdom with us during this research.

Authors contributions

Writing – original draft: XRZ, GL; Writing – review & editing: JV, AL, HV, GL, XRZ; Conceptualization: GL, AS, HV, JV, XRZ; Software: XRZ, DL, AL, AS, GL; Visualization: XRZ, GL, JV

References

Ahrens J, Geveci B, Law C. 2005. Paraview: An end-user tool for large data visualization. *The visualization handbook* 717.

Almeida AM, Silva AB, Araújo SS, Cardoso LA, Fevereiro PS. 2007. Responses to water withdrawal of tobacco plants genetically engineered with the AtTPS1 gene: A special reference to photosynthetic parameters. *Euphytica/ Netherlands journal of plant breeding* 154: 113–126.

Ayllón D, Grimm V, Attinger S, *et al.* 2018. Cross-disciplinary links in environmental systems science: Current state and claimed needs identified in a meta-review of process models. *The Science of the total environment* 622-623: 954–973.

Barczi J-F, Rey H, Caraglio Y, *et al.* 2008. AmapSim: a structural whole-plant simulator based on botanical knowledge and designed to host external functional models. *Annals of botany* 101: 1125–1138.

Bar-On YM, Phillips R, Milo R. 2018. The biomass distribution on Earth. *Proceedings of the National Academy of Sciences of the United States of America* 115: 6506–6511.

Barthélémy D, Caraglio Y. 2007. Plant architecture: a dynamic, multilevel and comprehensive approach to plant form, structure and ontogeny. *Annals of botany* 99: 375–407.

Bidel L, Pages L, Riviere LM, Pelloux G, Lorendeau JY. 2000. MassFlowDyn I: a carbon transport and partitioning model for root system architecture. *Annals of botany* 85: 869–886.

Boardman NK. 1977. Comparative Photosynthesis of Sun and Shade Plants. *Annual review of plant physiology* 28: 355–377.

Comtet J, Jensen KH, Turgeon R, Stroock AD, Hosoi AE. 2017. Passive phloem loading and long-distance transport in a synthetic tree-on-a-chip. *Nature plants* 3: 17032.

Da Silva D, Qin L, DeBuse C, DeJong TM. 2014. Measuring and modelling seasonal patterns of carbohydrate storage and mobilization in the trunks and root crowns of peach trees. *Annals of botany* 114: 643–652.

De Reffye P, Hu B-G. 2003. Relevant qualitative and quantitative choices for building an efficient dynamic plant growth model: GreenLab case In: *International Symposium on Plant Growth Modeling, Simulation, Visualization and their Applications-PMA'03*. Springer and Tsinghua University Press, 87–107.

De Schepper V, Steppe K. 2010. Development and verification of a water and sugar transport model using measured stem diameter variations. *Journal of experimental botany* 61: 2083–2099.

De Swaef T, De Schepper V, Vandegehuchte MW, Steppe K. 2015. Stem diameter variations as a versatile research tool in ecophysiology. *Tree physiology* 35: 1047–1061.

Doussan C, Pierret A, Garrigues E, Pagès L. 2006. Water uptake by plant roots: II--modelling of water transfer in the soil root-system with explicit account of flow within the root system--

comparison with experiments. *Plant and soil* 283: 99–117.

Draye X, Kim Y, Lobet G, Javaux M. 2010. Model-assisted integration of physiological and environmental constraints affecting the dynamic and spatial patterns of root water uptake from soils. *Journal of experimental botany* 61: 2145–2155.

Drouet J-L, Pagès L. 2003. GRAAL: a model of GRowth, Architecture and carbon ALlocation during the vegetative phase of the whole maize plant: model description and parameterisation. *Ecological modelling* 165: 147–173.

van Dusschoten D, Metzner R, Kochs J, *et al.* 2016. Quantitative 3D Analysis of Plant Roots Growing in Soil Using Magnetic Resonance Imaging. *Plant physiology* 170: 1176–1188.

Farquhar GD, von Caemmerer S, Berry JA. 2001. Models of photosynthesis. *Plant physiology* 125: 42–45.

Farrar JF, Jones DL. 2000. The control of carbon acquisition by roots: REVIEW Control of carbon acquisition by roots. *The New phytologist* 147: 43–53.

Fatichi S, Pappas C, Zscheischler J, Leuzinger S. 2019. Modelling carbon sources and sinks in terrestrial vegetation. *The New phytologist* 221: 652–668.

Fiorani F, Rascher U, Jahnke S, Schurr U. 2012. Imaging plants dynamics in heterogenic environments. *Current opinion in biotechnology* 23: 227–235.

Fiorani F, Schurr U. 2013. Future scenarios for plant phenotyping. *Annual review of plant biology* 64: 267–291.

Flemisch B, Darcis M, Erbertseder K, *et al.* 2011. DuMux: DUNE for multi-{phase,component,scale,physics,…} flow and transport in porous media. *Advances in water resources* 34: 1102–1112.

Garrigues E, Doussan C, Pierret A. 2006. Water uptake by plant roots: I - Formation and propagation of a water extraction front in mature root systems as evidenced by 2D light transmission imaging. *Plant and soil* 283: 83–98.

Heuvelink E. 1996. Dry Matter Partitioning in Tomato: Validation of a Dynamic Simulation Model. *Annals of botany* 77: 71–80.

Hui F, Zhu J, Hu P, *et al.* 2018. Image-based dynamic quantification and high-accuracy 3D evaluation of canopy structure of plant populations. *Annals of botany* 121: 1079–1088.

Hummel I, Pantin F, Sulpice R, *et al.* 2010. Arabidopsis plants acclimate to water deficit at low cost through changes of carbon usage: an integrated perspective using growth, metabolite, enzyme, and gene expression analysis. *Plant physiology* 154: 357–372.

Janott M, Gayler S, Gessler A, Javaux M, Klier C, Priesack E. 2011. A one-dimensional model of water flow in soil-plant systems based on plant architecture. *Plant and Soil* 341: 233–256.

Jasechko S, Sharp ZD, Gibson JJ, Birks SJ, Yi Y, Fawcett PJ. 2013. Terrestrial water fluxes dominated by transpiration. *Nature* 496: 347–350.

Javaux M, Schroeder T, Vanderborght J, Vereecken H. 2008. Use of a three-dimensional

detailed modeling approach for predicting root water uptake. *Vadose Zone Journal* 7: 1079–1088.

Jensen KH, Mullendore DL, Holbrook NM, Bohr T, Knoblauch M, Bruus H. 2012. Modeling the hydrodynamics of Phloem sieve plates. *Frontiers in plant science* 3: 151.

Jyske T, Hölttä T. 2015. Comparison of phloem and xylem hydraulic architecture in Picea abies stems. *The New phytologist* 205: 102–115.

Kallarackal J, Bauer SN, Nowak H, Hajirezaei M-R, Komor E. 2012. Diurnal changes in assimilate concentrations and fluxes in the phloem of castor bean (Ricinus communis L.) and tansy (Tanacetum vulgare L.). *Planta* 236: 209–223.

Kang MZ, Cournède PH, de Reffye P, Auclair D, Hu BG. 2008. Analytical study of a stochastic plant growth model: Application to the GreenLab model. *Mathematics and computers in simulation* 78: 57–75.

Knoblauch M, Knoblauch J, Mullendore DL, *et al.* 2016. Testing the Münch hypothesis of long distance phloem transport in plants. *eLife* 5.

Knoblauch J, Mullendore DL, Jensen KH, Knoblauch M. 2014. Pico gauges for minimally invasive intracellular hydrostatic pressure measurements. *Plant physiology* 166: 1271–1279.

Knoblauch M, Peters WS. 2017. What actually is the Münch hypothesis? A short history of assimilate transport by mass flow. *Journal of integrative plant biology* 59: 292–310.

Koch T, Heck K, Schröder N, Class H, Helmig R. 2018. A New Simulation Framework for Soil–Root Interaction, Evaporation, Root Growth, and Solute Transport. *Vadose Zone Journal* 17.

Lacointe A, Minchin PEH. 2008. Modelling phloem and xylem transport within a complex architecture. *Functional plant biology: FPB* 35: 772–780.

Lacointe A, Minchin PEH. 2019. A Mechanistic Model to Predict Distribution of Carbon Among Multiple Sinks In: Liesche J, ed. *Phloem: Methods and Protocols*. New York, NY: Springer New York, 371–386.

Leitner D, Klepsch S, Bodner G, Schnepf A. 2010. A dynamic root system growth model based on L-Systems. *Plant and soil* 332: 177–192.

Lichtenthaler HK, Buschmann C, Döll M, *et al.* 1981. Photosynthetic activity, chloroplast ultrastructure, and leaf characteristics of high-light and low-light plants and of sun and shade leaves. *Photosynthesis research* 2: 115–141.

Lobet G, Couvreur V, Meunier F, Javaux M, Draye X. 2014. Plant water uptake in drying soils. *Plant physiology* 164: 1619–1627.

Lobet G, Draye X. 2013. Novel scanning procedure enabling the vectorization of entire rhizotron-grown root systems. *Plant methods* 9: 1.

Lobet G, Hachez C, Chaumont F, Javaux M, Draye X. 2013. Root water uptake and water flow in the soil-root domain.

Lobet G, Paez-Garcia A, Schneider H, Junker A, Atkinson JA, Tracy S. 2019. Demystifying

roots: A need for clarification and extended concepts in root phenotyping. *Plant science: an international journal of experimental plant biology* 282: 11–13.

Lobet G, Pagès L, Draye X. 2012. A modeling approach to determine the contribution of plant hydraulic conductivities on the water uptake dynamics in the soil-plant-atmosphere system In: *2012 IEEE 4th International Symposium on Plant Growth Modeling, Simulation, Visualization and Applications*.235–241.

Lobet G, Pagès L, Draye X. 2014. A modeling approach to determine the importance of dynamic regulation of plant hydraulic conductivities on the water uptake dynamics in the soil-plant-atmosphere system. *Ecological modelling* 290: 65–75.

Lobet G, Pound MP, Diener J, *et al.* 2015. Root system markup language: toward a unified root architecture description language. *Plant physiology* 167: 617–627.

Lopez G, Favreau RR, Smith C, Costes E, Prusinkiewicz P, DeJong TM. 2008. Integrating simulation of architectural development and source--sink behaviour of peach trees by incorporating Markov chains and physiological organ function submodels into L-PEACH. *Functional plant biology: FPB* 35: 761–771.

Lynch JP. 2013. Steep, cheap and deep: an ideotype to optimize water and N acquisition by maize root systems. *Annals of botany* 112: 347–357.

Marcelis LFM. 1996. Sink strength as a determinant of dry matter partitioning in the whole plant. *Journal of experimental botany* 47: 1281–1291.

Marshall-Colon A, Long SP, Allen DK, *et al.* 2017. Crops In Silico: Generating Virtual Crops Using an Integrative and Multi-scale Modeling Platform. *Frontiers in plant science* 8: 786.

Martínez-Vilalta J, Prat E, Oliveras I, Piñol J. 2002. Xylem hydraulic properties of roots and stems of nine Mediterranean woody species. *Oecologia* 133: 19–29.

Mencuccini M, Manzoni S, Christoffersen B. 2019. Modelling water fluxes in plants: from tissues to biosphere. *The New phytologist* 222: 1207–1222.

Metz B, Davidson O, De Coninck H, Loos M, Meyer L. 2005. *IPCC special report on carbon dioxide capture and storage*. Intergovernmental Panel on Climate Change, Geneva (Switzerland). Working ….

Meunier F, Javaux M, Couvreur V, *et al.* 2016. RSWMS: a modelling platform to decipher soil-plant relations In: *Hacking the boundaries: event in multi-scale biological modelling*.

Minchin PEH, Lacointe A. 2017. Consequences of phloem pathway unloading/reloading on equilibrium flows between source and sink: a modelling approach. *Functional plant biology: FPB* 44: 507–514.

Mullendore DL, Windt CW, Van As H, Knoblauch M. 2010. Sieve tube geometry in relation to phloem flow. *The Plant cell* 22: 579–593.

Muller B, Pantin F, Génard M, *et al.* 2011. Water deficits uncouple growth from photosynthesis, increase C content, and modify the relationships between C and growth in sink organs. *Journal of experimental botany* 62: 1715–1729.

Münch E, b. 1930. Stoffbewegungen in der Pflanze.

Pincebourde S, Sinoquet H, Combes D, Casas J. 2007. Regional climate modulates the canopy mosaic of favourable and risky microclimates for insects. *The Journal of animal ecology* 76: 424–438.

Pokhilko Alexandra, Ebenhöh Oliver. 2015. Mathematical modelling of diurnal regulation of carbohydrate allocation by osmo-related processes in plants. *Journal of the Royal Society, Interface / the Royal Society* 12: 20141357.

Pradal C, Dufour-Kowalski S, Boudon F, Fournier C, Godin C. 2008. OpenAlea: a visual programming and component-based software platform for plant modelling. *Functional plant biology: FPB* 35: 751–760.

de Pury DGG, Farquhar GD. 1997. Simple scaling of photosynthesis from leaves to canopies without the errors of big-leaf models. *Plant, cell & environment* 20: 537–557.

Rellán-Álvarez R, Lobet G, Dinneny JR. 2016. Environmental Control of Root System Biology. *Annual review of plant biology* 67: 619–642.

Rellán-Álvarez R, Lobet G, Lindner H, *et al.* 2015. GLO-Roots: an imaging platform enabling multidimensional characterization of soil-grown root systems. *eLife* 4.

Savage JA, Beecher SD, Clerx L, *et al.* 2017. Maintenance of carbohydrate transport in tall trees. *Nature plants* 3: 965–972.

Savage JA, Clearwater MJ, Haines DF, *et al.* 2016. Allocation, stress tolerance and carbon transport in plants: how does phloem physiology affect plant ecology? *Plant, cell & environment* 39: 709–725.

Savage JA, Zwieniecki MA, Holbrook NM. 2013. Phloem transport velocity varies over time and among vascular bundles during early cucumber seedling development. *Plant physiology* 163: 1409–1418.

Schnepf A, Leitner D, Landl M, *et al.* 2018. CRootBox: a structural–functional modelling framework for root systems. *Annals of botany* 121: 1033–1053.

Schröder T, Javaux M, Vanderborght J, Körfgen B, Vereecken H. 2008. Effect of Local Soil Hydraulic Conductivity Drop Using a Three-Dimensional Root Water Uptake Model. *Vadose Zone Journal* 7: 1089–1098.

Seleznyova AN, Hanan J. 2018. Mechanistic modelling of coupled phloem/xylem transport for L-systems: combining analytical and computational methods. *Annals of botany*.

Sellin A. 1993. Resistance to water flow in xylem of Picea abies (L.) Karst. trees grown under contrasting light conditions. *Trees* 7: 220–226.

Sievänen R, Godin C, DeJong TM, Nikinmaa E. 2014. Functional-structural plant models: a growing paradigm for plant studies. *Annals of botany* 114: 599–603.

Sinoquet H, Le Roux X, Adam B, Ameglio T, Daudet FA. 2001. RATP: a model for simulating the spatial distribution of radiation absorption, transpiration and photosynthesis within canopies: application to an isolated tree crown. *Plant, cell & environment* 24: 395–406.

Steppe K, Sterck F, Deslauriers A. 2015. Diel growth dynamics in tree stems: linking anatomy and ecophysiology. *Trends in plant science* 20: 335–343.

Steudle E. 2001. THE COHESION-TENSION MECHANISM AND THE ACQUISITION OF WATER BY PLANT ROOTS. *Annual review of plant physiology and plant molecular biology* 52: 847–875.

Stitt M, Lunn J, Usadel B. 2010. Arabidopsis and primary photosynthetic metabolism - more than the icing on the cake. *The Plant Journal* 61: 1067–1091.

Streb S, Zeeman SC. 2012. Starch metabolism in Arabidopsis. *The Arabidopsis book / American Society of Plant Biologists* 10: e0160.

Thompson MV, Wolniak SM. 2008. A plasma membrane-anchored fluorescent protein fusion illuminates sieve element plasma membranes in Arabidopsis and tobacco. *Plant physiology* 146: 1599–1610.

Thorpe MR, Lacointe A, Minchin PEH. 2011. Modelling phloem transport within a pruned dwarf bean: a 2-source-3-sink system. *Functional plant biology: FPB* 38: 127.

Trenberth KE, Smith L, Qian T, Dai A, Fasullo J. 2007. Estimates of the Global Water Budget and Its Annual Cycle Using Observational and Model Data. *Journal of Hydrometeorology* 8: 758–769.

Tuzet A, Perrier A, Leuning R. 2003. A coupled model of stomatal conductance, photosynthesis and transpiration. *Plant, cell & environment* 26: 1097–1116.

Tyree MT. 1997. The Cohesion-Tension theory of sap ascent: current controversies. *Journal of experimental botany* 48: 1753–1765.

Van Bel AJE. 2003. The phloem, a miracle of ingenuity. *Plant, cell & environment* 26: 125–149.

Vereecken H, Huisman J-A, Franssen HJH, *et al.* 2015. Soil hydrology: Recent methodological advances, challenges, and perspectives. *Water resources research* 51: 2616–2633.

Vos J, Evers JB, Buck-Sorlin GH, Andrieu B, Chelle M, de Visser PHB. 2010. Functional-structural plant modelling: a new versatile tool in crop science. *Journal of experimental botany* 61: 2101–2115.

Website 1: https://www6.ara.inra.fr/piaf/Methodes-et-Modeles/PiafMunch

Website 2: https://colab.research.google.com/github/Plant-Root-Soil-Interactions-Modelling/CPlantBox/blob/isp/tutorial/jupyter/CPlantBox_PiafMunch_Tutorial_(include_installation).ipynb

William JHH, Minchin PEH, Farrar JF. 1991. Carbon Partitioning in Split Root Systems of Barley: The Effect of Osmotica. *Journal of experimental botany* 42: 453–460.

Windt CW, Vergeldt FJ, de Jager PA, van As H. 2006. MRI of long-distance water transport: a comparison of the phloem and xylem flow characteristics and dynamics in poplar, castor bean, tomato and tobacco. *Plant, cell & environment* 29: 1715–1729.

Wullschleger SD, Wilson KB, Hanson PJ. 2000. Environmental control of whole-plant

transpiration, canopy conductance and estimates of the decoupling coefficient for large red maple trees. *Agricultural and Forest Meteorology* 104: 157–168.

Xu L, Henke M, Zhu J, Kurth W, Buck-Sorlin G. 2011. A functional–structural model of rice linking quantitative genetic information with morphological development and physiological processes. *Annals of botany* 107: 817–828.

Yong ZHANG NZ. 2018. Imaging technologies for plant high-throughput phenotyping: a review. *Frontiers of Agricultural Science and Engineering* 5: 406–419.

Zhang L, Copini P, Weemstra M, Sterck F. 2016. Functional ratios among leaf, xylem and phloem areas in branches change with shade tolerance, but not with local light conditions, across temperate tree species. *The New phytologist* 209: 1566–1575.

Zhu X-G, Long SP, Ort DR. 2010. Improving photosynthetic efficiency for greater yield. *Annual review of plant biology* 61: 235–261.

Zhu X-G, Lynch JP, LeBauer DS, Millar AJ, Stitt M, Long SP. 2016. Plants in silico: why, why now and what?—an integrative platform for plant systems biology research. *Plant, cell & environment* 39: 1049–1057.

Zwieniecki MA, Melcher PJ, Michele Holbrook NM. 2001. Hydrogel control of xylem hydraulic resistance in plants. *Science* 291: 1059–1062.